Eur. Phys. J. A (2019) **55**: 27
DOI 10.1140/epja/i2019-12698-1

THE EUROPEAN PHYSICAL JOURNAL A

Regular Article – Experimental Physics

Activation cross-sections for the ^{185}Re(n, 2n) reaction and the isomeric cross-section ratio of ^{184m,g}Re in the neutron energy range of 13–15 MeV

Junhua Luo[1,2,a] and Li Jiang[3]

[1] Institute of New Energy, Hexi University, Zhangye 734000, China
[2] School of Physics and Electromechanical Engineering, Hexi University, Zhangye 734000, China
[3] Institute of Nuclear Physics and Chemistry, Chinese Academy of Engineering Physics, Mianyang 621900, China

Received: 18 November 2018 / Revised: 25 December 2018
Published online: 25 February 2019

Communicated by P. Capel

Abstract. Cross-sections and their isomeric ratios (σ_m/σ_g) for the ^{185}Re(n, 2n)^{184m}Re and ^{185}Re(n, 2n)^{184g}Re reactions in the 13–15 MeV range were measured. The neutron activation technique was applied using the K-400 neutron generator at the Chinese Academy of Engineering Physics (CAEP). Natural Re samples and Nb monitor foils were activated jointly to determine the reaction cross-section and the incident neutron flux. The ^{3}H(d, n)^{4}He reaction was used to generate the neutron beam. The pure cross-section of the ground state was derived from the absolute cross-section of the metastable state using residual nuclear decay analysis. Numerical calculations using the nuclear-model-based computer code TALYS-1.8 with six level density models were used to obtain ^{185}Re(n, 2n)^{184m,g}Re reaction excitation functions and their isomeric cross-section ratios. Finally, experimentally determined cross-sections were compared with corresponding literature data.

1 Introduction

Rhenium (Re) metal is a high temperature corrosion resistant material, and its boron-based alloys are effective neutron absorbers used in the regulation of nuclear reactors. A high output of 14 MeV neutrons can be achieved via the ^{3}H(d, n)^{4}He reaction, with a flux rate of approximately 3×10^{14} n/s [1]. As a result, the activation of structural materials in fusion reactors has to be considered. 14 MeV neutrons can induce a series of nuclear reactions including ^{185}Re(n, 2n)^{184m}Re, ^{185}Re(n, 2n)^{184g}Re and ^{185}Re(n, 2n)$^{184m+g}$Re, and the related cross-sectional data are of great importance for the evaluation of safety in fusion reactors. In particular, they can be used to determine the required treatment of radioactive waste from reactor structural materials and improve radiation protection procedures.

In the neutron-induced ^{185}Re(n, 2n) reaction, the isomeric state of the produced nuclei has a long half-life (^{184m}Re, $T_{1/2} = 169$ d, ^{184g}Re, $T_{1/2} = 35.4$ d). After isomeric transition (IT), the excited state can affect the activity of the ground state, and gamma rays generated after electron capture (EC) in the excited state coincide with the main characteristic rays in the ground state (see fig. 1) [2]. This adds complexity to the measurement of the cross-section of the pure ^{185}Re(n, 2n)^{184g}Re reaction. In the 13–15 MeV energy region, there is significant inconsistency in published data regarding the ^{185}Re(n, 2n)^{184m}Re, ^{185}Re(n, 2n)^{184g}Re and ^{185}Re(n, 2n)$^{184m+g}$Re reactions. For the ^{185}Re(n, 2n)^{184m}Re reaction, the value of the cross-section in ref. [3] is more than 2.5 times greater than the values reported in refs. [4–9]. For the ^{185}Re(n, 2n)^{184g}Re reaction, the cross-sections described in refs. [3, 5–7] are around 1800 mb, while the values from refs. [4, 8, 9] are around 1400 mb. The results regarding the ^{185}Re(n, 2n)$^{184m+g}$Re reaction given in refs. [5–7] are almost 30% higher than those in refs. [4, 8–10], and the value in ref. [3] is even higher (about 3000 mb).

Discrepancies in the literature mentioned above may be due to the following two reasons. The first is related to difference in decay data (*i.e.*, the selection of characteristic rays). As shown in fig. 1, the main characteristic rays of the produced nuclei in the ^{185}Re(n, 2n)^{184m,g}Re reactions are partly coincident. However, the procedure for eliminating these effects is not found in the published literature. The second pertains to the interference reaction processing method. In the ^{185}Re(n, 2n)^{184g}Re reaction, the effects of both IT and EC of ^{184m}Re on ^{184g}Re should be

[a] e-mail: luojh71@163.com (corresponding author)

Table 1. Summary of ^{185}Re(n, 2n) reaction cross-sections from previous measurements.

Reaction	Decay data	Detector	Monitor reaction	Reference
^{185}Re(n, 2n)^{184m}Re	$T_{1/2} = 2.2$ d		^{197}Au(n, 2n)^{196}Au	Ref. [3]
	$T_{1/2} = 169$ d, $E\gamma = 104.73$ keV, $I\gamma = 13.73\%$	HPGe	^{93}Nb(n, 2n)^{92m}Nb	Ref. [4]
	$T_{1/2} = 169$ d, $E\gamma = 920.933$ keV, $I\gamma = 8.133\%$		No information	Ref. [5]
	$T_{1/2} = 169$ d, $E\gamma = 104.7$ keV, $I\gamma = 13.4\%$	GeLi	^{93}Nb(n, 2n)^{92m}Nb	Ref. [6]
	$T_{1/2} = 169$ d, $E\gamma = 920.93$ keV, $I\gamma = 8.2\%$	HPGe	^{27}Al(n, α)^{24}Na	Ref. [7]
	$E\gamma = 895$ keV, $I\gamma = 14.8\%$; $E\gamma = 904$ keV, $I\gamma = 44.5\%$	PROPC	No information	Ref. [8]
	$T_{1/2} = 169$ d, $E\gamma = 104.7$ keV ($I\gamma = 13.6\%$), $E\gamma = 161.3$ keV ($I\gamma = 6.56\%$), $E\gamma = 563.7$ keV ($I\gamma = 3.33\%$), $E\gamma = 920.9$ keV ($I\gamma = 8.2\%$)	HPGe	^{93}Nb(n, 2n)^{92m}Nb	Ref. [9]
^{185}Re(n, 2n)^{184g}Re	$T_{1/2} = 50$ d		^{197}Au(n, 2n)^{196}Au	Ref. [3]
	$T_{1/2} = 38.0$ d, $E\gamma = 112.07$ keV, $I\gamma = 17.21\%$	HPGe		Ref. [4]
	$T_{1/2} = 38.0$ d, $E\gamma = 903.282$ keV, $I\gamma = 37.88\%$	HPGe	^{93}Nb(n, 2n)^{92m}Nb	Ref. [5]
	$T_{1/2} = 38.0$ d, $E\gamma = 641.9$ keV, $I\gamma = 1.936\%$	GeLi	^{93}Nb(n, 2n)^{92m}Nb	Ref. [6]
	$T_{1/2} = 38.0$ d, $E\gamma = 792.07$ keV $I\gamma = 37.7\%$	HPGe	^{27}Al(n, α)^{24}Na	Ref. [7]
	$T_{1/2} = 35.4$ d, $E\gamma = 792.1$ keV ($I\gamma = 37.7\%$), $E\gamma = 894.8$ keV ($I\gamma = 15.7\%$), $E\gamma = 903.3$ keV ($I\gamma = 38.1\%$)	HPGe	^{93}Nb(n, 2n)^{92m}Nb	Ref. [9]

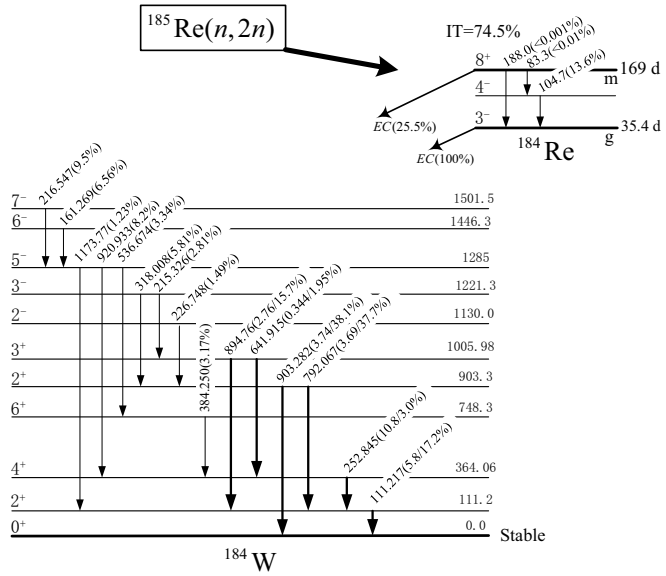

Fig. 1. Metastable and ground states in the ^{185}Re(n, 2n)^{184m,g}Re reactions [2]. All energies are in keV. Transition from both the excited and ground state is represented by the bold black line, with the intensity in brackets indicating rays originating from both states.

eliminated. Nevertheless, the elimination of these effects has not been addressed in detail in previous studies.

Thus, in this study we utilize the latest decay data and the related decay laws of the produced nuclei to remove the effect of interference reactions and select multiple appropriate characteristic rays. We then calculate the weighted average of the cross-section of the ^{185}Re(n, 2n)^{184m}Re reaction and the ^{185}Re(n, 2n)^{184g}Re reaction in the pure ground state and the related cross-section ratio. The obtained cross-sections are then analyzed in comparison with theoretical and previously reported results (table 1).

2 Experimental

2.1 Material

Disk of natural rhenium metal (purity 99.99%, about 1.0 mm in thickness, 2.0 cm in diameter, China New Metal Materials Technology Co, Ltd.) was sandwiched between disks of niobium (purity 99.99%, 0.12 mm in thickness) of the same diameter. Three such samples (Nb-Re-Nb) were prepared for irradiation.

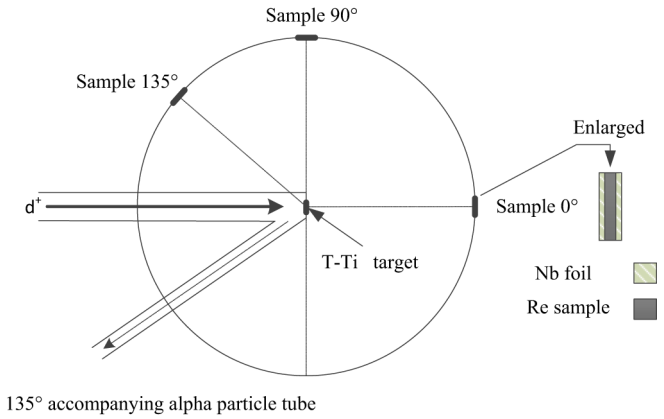

Fig. 2. Sketch of the experimental geometry.

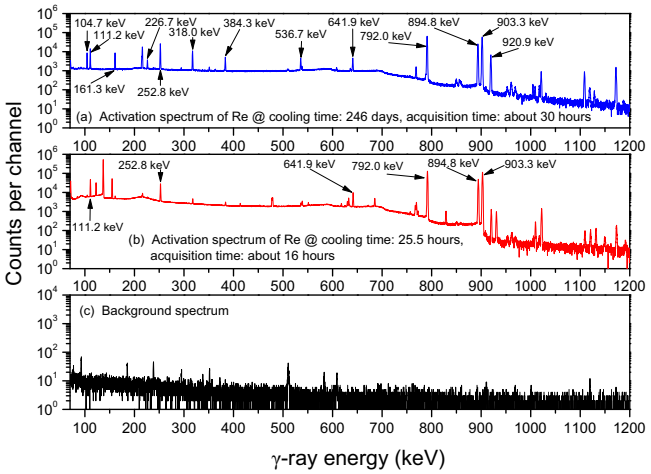

Fig. 3. (a) γ-ray spectrum of rhenium obtained after 246 days of cooling from the end of irradiation; acquisition time: about 30 hours. (b) γ-ray spectrum of rhenium obtained after 25.5 hours of cooling from the end of irradiation, acquisition time: about 16 hours; (c) Background spectrum.

2.2 Neutron energy and irradiation

The irradiation of the rhenium disks was performed at the Chinese Academy of Engineering Physics (CAEP) K-400 neutron generator. A beam with an effective deuteron beam energy of 136 keV and current of 260 μA was used for the production of neutrons via the ^{3}H(d, n)^{4}He reaction. The neutron-production target was a tritium-titanium (T-Ti) target 2.20 mg cm^{-2} in thickness. The neutron yield was $\sim$ (3–4) $\times$ 10^{10}n/(4πs). The sample positions in the experiment are shown in fig. 2. Groups of samples were placed at 0°, 90° or 135° with respect to the beam line and centered about the T-Ti target at distances of about 40 mm. Natural Re samples and Nb monitor foils were activated jointly to determine the reaction cross-section and the incident neutron flux. Further details can be found in our previously published work [11–13]. Neutron energies in this measurement were obtained using the formula from ref. [14], which is determined by the distance between the sample and T-Ti target, the emergent angle and the radius of the sample.

2.3 Gamma spectroscopic measurements

The activities of product radionuclides were measured using high-purity germanium (HPGe) gamma-ray spectroscopy ($\sim$ 68% relative efficiency, 1.69 keV resolution at 1332.5 keV of ^{60}Co). The detector was connected to a digital gamma spectrometry system (ORTEC, model GEM 60P) and Maestro data acquisition software. The separation between sample and detector was variable within a range of 0 to 8 cm. Figure 3 shows the typical spectra acquired from the irradiated Re samples during measurement of isomeric and ground states, with the γ-rays of interest marked. The γ-ray intensities and half-lives used in the analysis are summarized in table 2 [2].

2.4 Calculation of cross-sections and their uncertainties

The method for cross-section calculation is described in detail in our previous papers [15,16]. The standard activation equation was employed:

$$\sigma_x = \frac{[S\varepsilon I_\gamma \eta K M D]_0}{[S\varepsilon I_\gamma \eta K M D]_x} \cdot \frac{[\lambda A F C]_x}{[\lambda A F C]_0} \sigma_0, \tag{1}$$

where F is the total correction factor of the activity, given by

$$F = f_s \times f_c, \tag{2}$$

where f_s and f_c are the correction factors for the self-absorption of the sample at a given gamma energy, and the coincidence sum effect of cascade gamma rays in the investigated nuclide, respectively.

Rhenium is a heavy element with very pronounced gamma ray self-absorption, particularly at low energies. Values of the mass attenuation coefficient (μ/ρ) for rhenium were obtained by interpolating the values reported in [17]. Correction factors for the characteristic gamma-ray levels are given in table 3.

In the process of calculating the cross-sections of the ^{185}Re(n, 2n)^{184g}Re reactions, C_x in eq. (1) should be the result of the measured full-energy peak area minus the contribution from ^{184m}Re via ^{184m}Re $\xrightarrow{\text{IT}(74.5\%)}$ ^{184g}Re (C_1) and via ^{184m}Re $\xrightarrow{\text{EC}(25.5\%)}$ ^{184}W(C_2). Rules for the creation and decay of artificial radioactive nuclides (see [15,16] for details) provide that C_1 and C_2 can be written as

$$C_1 = \frac{P_{mg}\varepsilon_g I_g C_m(\lambda_g^2 S_m D_m - \lambda_m^2 S_g D_g)}{(\lambda_g - \lambda_m) S_m D_m I_m \varepsilon_m \lambda_g K_m}, \tag{3}$$

$$C_2 = \frac{\varepsilon_{m2} I_{\gamma 2} C_{m1}}{\varepsilon_{m1} I_{\gamma 1}}, \tag{4}$$

where m, g, P_{mg}, C_m, I and ε are metastable state, ground state, fraction of metastable state decays that produce ground state nuclides (branching ratio), full energy peak

Table 2. Measured nuclear reactions on rhenium and decay data (taken from [2]). The boldface font is used in the calculation.

Reaction	Abundance of target isotope (%)	Half-life of product	E-threshold (MeV)	Mode of decay (%)	$E\gamma$ (keV)	$I\gamma$ (%)
^{185}Re(n, 2n)^{184m}Re	37.40_2	169 d_8	7.900	IT(74.50)	**104.739**	**13.6$_4$**
				EC(25.50)	111.217	5.8_4
					161.269	**6.56$_{24}$**
					226.748	**1.49$_6$**
					252.845	10.8_4
					318.008	**5.81$_{20}$**
					384.250	**3.17$_{11}$**
					536.674	**3.34$_{12}$**
					641.915	0.344_{16}
					792.067	3.69_{14}
					894.760	2.76_{13}
					903.282	3.74_{14}
					920.933	**8.2$_3$**
^{185}Re(n, 2n)^{184g}Re	37.40_2	35.4 d_7	7.711	EC(100)	**111.217**	**17.2$_7$**
					252.845	**3.0$_3$**
					641.915	**1.95$_6$**
					792.067	**37.7$_{11}$**
					894.760	**15.7$_5$**
					903.282	**38.1$_{12}$**
^{93}Nb(n, 2n)^{92m}Nb	100	10.15 d_2	8.972	EC(100)	934.44	99.15_4

area of the measured metastable state, gamma ray intensity and full-energy peak efficiency of the characteristic gamma-rays, respectively.

S_m, S_g, D_m and D_g are given by

$$\begin{aligned} S_m &= 1 - e^{-\lambda_m T}, \\ S_g &= 1 - e^{-\lambda_g T}, \\ D_m &= e^{-\lambda_m t_1} - e^{-\lambda_m t_2}, \\ D_g &= e^{-\lambda_g t_1} - e^{-\lambda_g t_2}. \end{aligned}$$

In eq. (4), the subscript 1 and 2 represent two different characteristics of gamma rays.

3 Experimental uncertainty

3.1 Mean (arithmetic average)

The relation for experimental mean σ for n trial measurements, $\sigma_i \pm \Delta\sigma_i$, with $i = 1, \ldots, n$, is given by

$$\sigma = \frac{\sum_{i=1}^{n}[\sigma_i/(\Delta\sigma_i)^2]}{\sum_{i=1}^{n}[1/(\Delta\sigma_i)^2]}\,. \tag{5}$$

3.2 Experimental standard deviation

The experimental standard deviation $\Delta\sigma_A$ is defined as

$$\Delta\sigma_A = \left[\frac{\sum_{i=1}^{n}[(\sigma_i - \sigma)^2/(\Delta\sigma_i)^2]}{(n-1)\sum_{i=1}^{n}[1/(\Delta\sigma_i)^2]}\right]^{1/2}. \tag{6}$$

Obtaining as much knowledge as possible from a limited number of measurements is one of the fundamental problems in experimental science. In particular, eq. (6) for the error $\Delta\sigma_A$ of the weighted mean can yield unphysical values for very small samples.

In order to prevent this, we introduce $\Delta\sigma_B$ which limits the contribution of individual errors to $\Delta\sigma$

$$\Delta\sigma_B = \left[\sum_{i=1}^{n}\frac{1}{(\Delta\sigma_i)^2}\right]^{-1/2}. \tag{7}$$

However, eq. (7) may also fail if two data points are very different and have relatively small error bars. The standard deviation $\Delta\sigma$ of the weighted average σ may then be calculated for a limited number of measurements using the following equation:

$$\Delta\sigma = \max(\Delta\sigma_A, \Delta\sigma_B). \tag{8}$$

Table 3. Correction factors for the self-absorption of the sample at a given gamma-ray energy.

Gamma-ray energy (keV)	μ/ρ (cm^2/g)	μ (cm^{-1})	Samples		Correction factors f_s
			No.	Thickness h (cm)	
104.739	4.3074	90.542	1	0.0984	8.910
			2	0.0973	8.811
			3	0.0939	8.504
111.217	3.9252	82.508	1	0.0984	8.121
			2	0.0973	8.031
			3	0.0939	7.751
161.269	1.4510	30.501	1	0.0984	3.158
			2	0.0973	3.129
			3	0.0939	3.037
226.748	0.6840	14.379	1	0.0984	1.869
			2	0.0973	1.858
			3	0.0939	1.823
252.845	0.5593	11.757	1	0.0984	1.688
			2	0.0973	1.679
			3	0.0939	1.652
318.008	0.3094	6.503	1	0.0984	1.354
			2	0.0973	1.349
			3	0.0939	1.336
384.250	0.2191	4.605	1	0.0984	1.244
			2	0.0973	1.241
			3	0.0939	1.232
536.674	0.1301	2.734	1	0.0984	1.141
			2	0.0973	1.139
			3	0.0939	1.134
641.915	0.1052	2.211	1	0.0984	1.113
			2	0.0973	1.111
			3	0.0939	1.107
792.067	0.0830	1.744	1	0.0984	1.088
			2	0.0973	1.087
			3	0.0939	1.084
894.760	0.0747	1.571	1	0.0984	1.079
			2	0.0973	1.078
			3	0.0939	1.076
903.282	0.0741	1.557	1	0.0984	1.079
			2	0.0973	1.078
			3	0.0939	1.075
920.933	0.0728	1.530	1	0.0984	1.077
			2	0.0973	1.076
			3	0.0939	1.074

Uncertainty analysis was carried out using the quadrature method [18]. The uncertainties quoted for the present measurements are estimates of standard uncertainties and include contributions due to uncertainties in cross-section of the monitor reaction (1.1–1.5%), photopeak detection efficiency (2.0–3.0%), counting statistics (0.04–2.0%), relative gamma-ray intensity (0.1–10.0%), half-life (0.02–4.7%), sample weight (< 0.1%), timing (< 0.1%), self-absorption of gamma-ray (∼ 0.5%), and isotopic abundance (0.06%). The uncertainty of the weighted average cross-section was between 3.2 and 4.4%.

4 Nuclear model calculations

Nuclear model-based calculations are of great importance since the existing measured data on cross-sections induced by neutrons for the evaluation of safety in fusion reactors are lacking or inconsistent. It is well known that nuclear reaction models are reliable means for calculating the energy and angle distributions of the reaction products or radionuclide production cross-sections [19,20]. The reaction model calculations include direct-interaction, equilibrium and pre-equilibrium processes. Level density as a function of energy is among the most important inputs for cross-section calculation within nuclear reaction models [21]. Nuclear level density (NLD) is the number of excited levels per energy interval ($\mathrm{d}N/\mathrm{d}E$) near the excitation energy. Excited nuclear levels are discrete at low energies; however, they approach a continuum as the excitation energy increases. Therefore, a nuclear model for calculating level density is needed for the continuum energy regime. An accurate and reliable description of the excited levels of a nucleus at both low and high excitation energy region is necessary for testing the quality of a reaction model used for the calculation of cross-sections [22]. The TALYS code (version 1.8) calculates the partial and total cross-section, the angular distribution, the energy spectrum, the differential spectrum and recoils. This code employs various microscopic and phenomenological nuclear level density models for obtaining the nuclear cross-sections [23]. The theoretical excitation function of the $^{185}\mathrm{Re}(\mathrm{n},2\mathrm{n})^{184\mathrm{m}}\mathrm{Re}$ and $^{185}\mathrm{Re}(\mathrm{n},2\mathrm{n})^{184\mathrm{g}}\mathrm{Re}$ reactions and their isomeric cross-section ratios at different neutron energies from threshold to 20 MeV were calculated using TALYS, with default values of the parameters and only the selected level density parameters adjusted. The details of the level density parameters were reported elsewhere [11,12,24–26].

5 Results and discussion

Cross-sections measured across the energy range of 13 to 15 MeV are given in table 4. The results obtained are prone to relatively small uncertainties due to the use of the weighted average method. All the nuclear reactions investigated within the scope of this work are discussed below. Cross-sections for the $^{93}\mathrm{Nb}(\mathrm{n},2\mathrm{n})^{92\mathrm{m}}\mathrm{Nb}$ monitor reaction were taken from ref. [27].

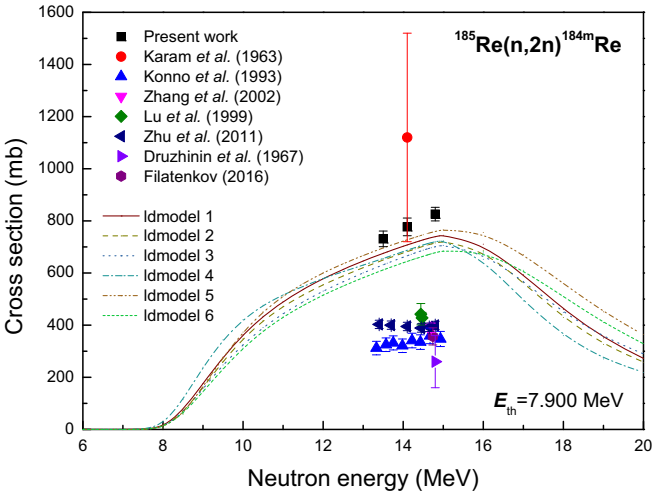

Fig. 4. Excitation functions of the $^{185}\mathrm{Re}(\mathrm{n},2\mathrm{n})^{184\mathrm{m}}\mathrm{Re}$ reaction for measured and literature data.

5.1 $^{185}\mathrm{Re}(\mathrm{n},2\mathrm{n})^{184\mathrm{m}}\mathrm{Re}$ reaction

In the present work, gamma-rays with energies of 104.7 keV (I_γ = 13.6%), 161.3 keV (I_γ = 6.56%), 226.7 keV (I_γ = 1.49%), 318.0 keV (I_γ = 5.81%), 384.3 keV (I_γ = 3.17%), 536.7 keV (I_γ = 3.34%), and 920.9 keV (I_γ = 8.2%) emitted in the decay of $^{184\mathrm{m}}\mathrm{Re}$ were used to calculate the value of the $^{185}\mathrm{Re}(\mathrm{n},2\mathrm{n})^{184\mathrm{m}}\mathrm{Re}$ reaction cross-section. In a previous measurement [8], the 895 keV and 904 keV gamma-rays were used to calculate the values of the $^{185}\mathrm{Re}(\mathrm{n},2\mathrm{n})^{184\mathrm{m}}\mathrm{Re}$ reaction cross-section. However, these two gamma-rays not only result from the product of $^{185}\mathrm{Re}(\mathrm{n},2\mathrm{n})^{184\mathrm{m}}\mathrm{Re}$ reaction, but also from the product of $^{185}\mathrm{Re}(\mathrm{n},2\mathrm{n})^{184\mathrm{g}}\mathrm{Re}$ reaction and the decay $^{184\mathrm{m}}\mathrm{Re} \xrightarrow{\mathrm{IT}(74.5\%)} {}^{184\mathrm{g}}\mathrm{Re}$. The threshold energy of this reaction is 7.900 MeV. In order to avoid the effect of low-energy neutrons, a reaction near the threshold, *i.e.* the $^{93}\mathrm{Nb}(\mathrm{n},2\mathrm{n})^{92\mathrm{m}}\mathrm{Nb}$ (E_{th} = 8.972 MeV) monitor reaction was selected, whereas Zhu *et al.* [7] used the lower threshold monitor reaction $^{27}\mathrm{Al}(\mathrm{n},\alpha)^{24}\mathrm{Na}$ (E_{th} = 3.249 MeV) and Zhang *et al.* [5] and Druzhinin *et al.* [8] did not give information about the monitor reaction. Figure 4 shows weighted averages of our results along with other published data from refs. [3–9]. It can be seen that there are significant differences among the data from the literature. In the energy region between 13 and 15 MeV the values of TALYS-1.8 calculation using ldmodels 1-6 are about 100% higher than the values from previous measurements [4–9], with the exception of Karam *et al.* [3]. Shapes of the excitation curves of the TALYS-1.8 calculation with ldmodels 1-6 exhibit a trend similar to the present data set, but the obtained results are somewhat higher than the theoretical calculations.

5.2 $^{185}\mathrm{Re}(\mathrm{n},2\mathrm{n})^{184\mathrm{g}}\mathrm{Re}$ reaction

Seven earlier measurements of the $^{185}\mathrm{Re}(\mathrm{n},2\mathrm{n})^{184\mathrm{g}}\mathrm{Re}$ reaction were published in [3–9]. In the present

Table 4. Measured cross-sections.

Reaction	$E\gamma$ (keV)	Cross-sections (in mb) at various neutron energies (in MeV)		
		13.5 ± 0.2	14.1 ± 0.2	14.8 ± 0.2
^{185}Re(n, 2n)^{184m}Re	104.739	840 ± 45	893 ± 47	910 ± 48
	161.269	766 ± 42	824 ± 45	859 ± 47
	226.748	678 ± 44	697 ± 45	769 ± 50
	318.008	692 ± 37	736 ± 39	784 ± 42
	384.250	648 ± 40	693 ± 43	759 ± 47
	536.674	685 ± 45	737 ± 48	793 ± 52
	920.933	850 ± 47	912 ± 50	926 ± 51
Weighted average ± standard uncertainty		731 ± 30	777 ± 34	826 ± 26
^{185}Re(n, 2n)^{184g}Re	111.217	1409 ± 120	1325 ± 113	1319 ± 112
	252.845	1399 ± 175	1352 ± 169	1237 ± 155
	641.915	1462 ± 107	1483 ± 108	1517 ± 111
	792.067	1526 ± 125	1524 ± 125	1567 ± 128
	894.760	1483 ± 126	1484 ± 126	1520 ± 129
	903.282	1468 ± 110	1468 ± 110	1505 ± 113
Weighted average ± standard uncertainty		1462 ± 50	1445 ± 49	1427 ± 63
^{185}Re(n, 2n)$^{184m+g}$Re		2193 ± 80	2222 ± 83	2253 ± 89
^{93}Nb(n, 2n)^{92m}Nb	934.44	457.9 ± 6.8 [27]	459.8 ± 6.8 [27]	459.7 ± 5.0 [27]

work, gamma-rays with energies of 111.217 keV (I_γ = (17.2 ± 0.7)%), 252.845 keV (I_γ = (3.0 ± 0.3)%), 641.915 keV (I_γ = (1.95 ± 0.06)%), 792.067 keV (I_γ = (37.7 ± 1.1)%), 894.76 keV (I_γ = (15.7 ± 0.5)%), and 903.282 keV (I_γ = (38.1 ± 1.2)%) emitted in the ^{184g}Re decay were used to calculate the values of the ^{185}Re(n, 2n)^{184g}Re reaction cross-section. The contribution of the ^{185}Re(n, 2n)^{184g}Re reaction via $^{184m}\text{Re} \xrightarrow{\text{IT}(74.5\%)} {}^{184g}\text{Re}$ and via $^{184m}\text{Re} \xrightarrow{\text{EC}(25.5\%)} {}^{184}\text{W}$ was subtracted using equations from refs. [3,4]. Figure 5 shows the excitation function of the ^{185}Re(n, 2n)^{184g}Re reaction. The ^{185}Re(n, 2n)^{184g}Re reaction cross-section data in the region from 13 to 15 MeV can be grouped into two bands differing by about 30%. The present results are in agreement with TALYS-1.8 calculations using ldmodels 1, 4, and 6 within experimental uncertainties, while the results by Karam *et al.* (1963) [3], Zhang *et al.* (2002) [5], Lu *et al.* (1999) [6], and Zhu *et al.* (2011) [7] are about 30% higher than the values of the present work, Konno *et al.* (1993) [4], Druzhinin *et al.* (1967) [8], Filatenkov (2016) [9], and TALYS-1.8 calculations with ldmodels 1-6.

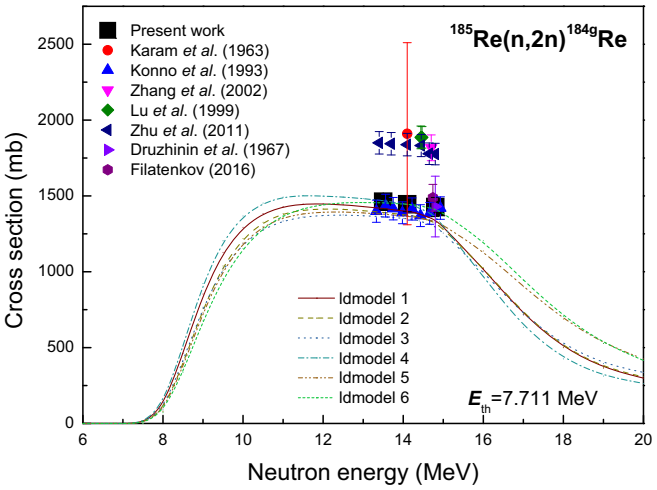

Fig. 5. Excitation function of the ^{185}Re(n, 2n)^{184g}Re reaction for measured and literature data.

5.3 ^{185}Re(n, 2n)$^{184m+g}$Re reaction

Figure 6 shows the data we obtained for the cross-section of ^{185}Re(n, 2n)$^{184m+g}$Re reaction together with TALYS-1.8 theoretical calculations using ldmodels 1-6, and previous measurements from refs. [4–10]. In the 13 to 15 MeV energy range, our data are consistent within the experimental uncertainties with results of Zhang *et al.* (2002) [5], Lu *et al.* (1999) [6], and Zhu *et al.* (2011) [7], but are higher than the results of refs. [4,8–10]. The determined excitation function follows this trend, which is characteristic for the ^{185}Re(n, 2n)$^{184m+g}$Re reaction, showing a plateau around 14 MeV and a decreasing trend with higher neutron energy.

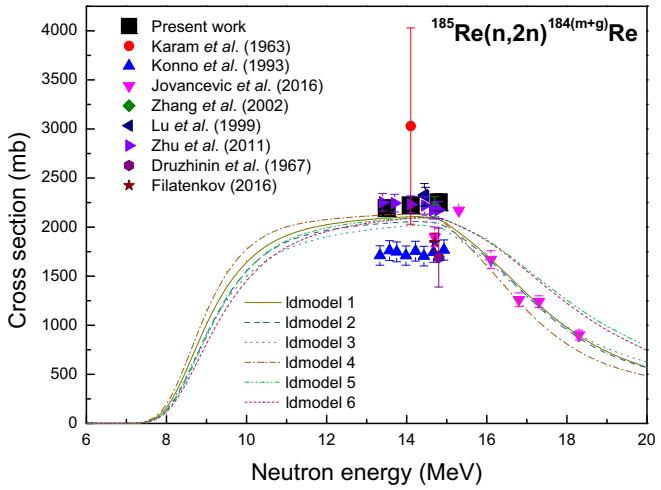

Fig. 6. Excitation function of the ^{185}Re(n, 2n)$^{184m+g}$Re reaction.

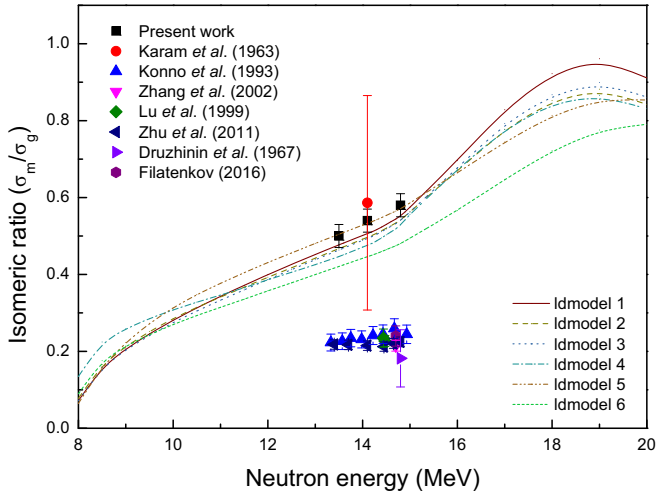

Fig. 7. Cross-section ratio of the ^{185}Re(n, 2n)^{184m}Re and ^{185}Re(n, 2n)^{184g}Re reactions as a function of the neutron energy.

5.4 Isomeric cross-section ratio of the ^{185}Re(n, 2n)^{184m,g}Re reactions

The cross-section ratio (σ_m/σ_g) for the isomeric pair ^{184m,g}Re produced in the (n,2n) reaction on ^{185}Re was found to be 0.50 ± 0.03, 0.54 ± 0.03, and 0.58 ± 0.3 at 13.5 ± 0.2, 14.1 ± 0.2 and 14.8 ± 0.2 MeV incident neutron energies, respectively. Figure 7 shows our experimental data together with the results of TALYS-1.8 numerical calculation using ldmodels 1-6. It can be seen that between 13 and 15 MeV our experimental results agree with the values from ref. [3] and TALYS-1.8 calculations using ldmodel 5 within their experimental uncertainty. However, they are exceeded by both the results published in refs. [4–9] and TALYS-1.8 calculations using ldmodel 1, 2, 3, 4, and 6. The isomeric cross-section ratio determined in this work shows an increasing trend with increasing neutron energy, suggesting that at higher excitation energies the formation of the high-spin isomer ($8^+ \rightarrow 3^-$) is favored. This trend is similar to several other neutron- and charged-particle-induced reactions near thresholds [28–37]. In the range of 13–15 MeV, the calculated isomeric cross-section ratio shows the same increasing trend for the six ldmodels.

6 Conclusion

The activation cross-sections for ^{185}Re(n, 2n)^{184m}Re, ^{185}Re(n, 2n)^{184g}Re, and ^{185}Re(n, 2n)$^{184m+g}$Re reactions along with isomeric cross-section ratios induced by 13.5, 14.1 and 14.8 MeV neutrons, have been obtained using the latest decay data and weighted average method. The nuclear model using the TALYS code showed that the microscopic level densities (Skyrme force) from Hilaire's combinatorial tables (ldmodel 5) [38] are appropriate for the isomeric cross-section ratios for ^{185}Re(n, 2n)^{184m}Re and ^{185}Re(n, 2n)^{184g}Re reactions, while models composed of microscopic level densities (Skyrme force) from Goriely's tables [38] (ldmodel 4) and microscopic level densities (temperature dependent HFB, Gogny force) from Hilaire's combinatorial tables [38] (ldmodel 6) are found to be appropriate for the ^{185}Re(n, 2n)^{184g}Re reaction. Our experimental results were then compared to those from the literature and to numerical calculations. The comparative analysis including cross-section data from the literature revealed that the inconsistencies in the published data can stem from: 1) the decay data (the selection of characteristic gamma-rays); 2) interfering reactions. A detailed comparison with theoretical calculations revealed that σ_g and σ_{m+g} cross-sections were easily reproduced by the calculations, while for σ_m (8^+), the theoretical results could only describe the general trend of the experimental data. Results reveal the importance of the level scheme of the residual nuclei and indicate the possibility of incomplete documentation of high-spin levels in the level schemes of these residual nuclei. Furthermore, they highlight certain limitations in the nuclear codes, particularly regarding the embedding of discrete states in the continuum, which is not currently possible and affects the reproduction of high-spin isomeric cross-sections. The results presented in this work are valuable for the improvement of nuclear data libraries, verification of nuclear reaction models and other practical applications.

We would like to thank the Intense Neutron Generator group at the Chinese Academy of Engineering Physics for performing the irradiations. This work was supported by the National Natural Science Foundation of China (Grant No. 11565012).

Data Availability Statement This manuscript has no associated data or the data will not be deposited. [Author's comment: All data generated during this study are contained in this published article.]

Publisher's Note The EPJ Publishers remain neutral with regard to jurisdictional claims in published maps and institutional affiliations.

References

1. Lynda L. Seaver, *World's largest laser sets records for neutron yield and laser energy* (Lawrence Livermore National Laboratory, 2010) `https://www.llnl.gov/news/worlds-largest-laser-sets-records-neutron-yield-and-laser-energy`.
2. Evaluated Nuclear Structure Data File (ENSDF), `http://www.nndc.bnl.gov/ensdf/`.
3. R.A. Karam, T.F. Parkinson, W.H. Ellis, *The Nuclear Properties of Rhenium*, Report, Dept. of Defence Reports (1963) No. 402668.
4. C. Konno *et al.*, Report, JAERI Reports (1993) No. 1329.
5. F. Zhang *et al.*, High Energy Phys. Nucl. Phys. **26**, 678 (2002) (Chinese ed.).
6. H. Lu *et al.*, At. Energy Sci. Technol. **33**, 410 (1999).
7. C. Zhu *et al.*, Nucl. Sci. Eng. **169**, 188 (2011).
8. A.A. Druzhinin, A.A. Lbov, L.P. Bilibin, Yad. Fiz. **5**, 18 (1967).
9. A.A. Filatenkov, Report, USSR report to the I.N.D.C. (2016) No. 0460.
10. N. Jovancevic *et al.*, Eur. Phys. A **52**, 148 (2016).
11. J. Luo *et al.*, Radiochim. Acta **105**, 779 (2017).
12. J. Luo, L. Jiang, Phys. Rev. C **96**, 044617 (2017).
13. J. Luo, L. Jiang, L. He, J. Radioanal. Nucl. Chem. **316**, 733 (2018).
14. J. Luo, L. Du, J. Zhao, Nucl. Instrum. Methods B **298**, 61 (2013).
15. J. Luo, L. Jiang, L. He, Phys. Rev. C **97**, 044617 (2018).
16. J. Luo, L. Jiang, X. Wang, Eur. Phys. A **54**, 67 (2018).
17. J.H. Hubbell, S.M. Seltzer, *Tables of x-ray mass attenuation coefficients and mass energy-absorption coefficients from 1* keV *to 20* MeV *for elements* $Z = 1$ *to 92 and 48 additional substances of dosimetric interest* (1996) `http://physics.nist.gov/PhysRefData/XrayMassCoef/tab3.html`.
18. J.R. Taylor, *An Introduction to Uncertainty Analysis* (University Science Books, Mill Valley, CA, 1982).
19. H. Korkut *et al.*, J. Fusion Energy **35**, 591 (2016).
20. M. Yiğit, E. Tel, İ.H. Sarpün, Nucl. Instrum. Methods B **385**, 59 (2016).
21. M. Yiğit, J. Fusion Energy **34**, 1392 (2015).
22. B. Canbula, Nucl. Instrum. Methods B **391**, 73 (2017).
23. A. Koning, S. Hilaire, S. Goriely, *TALYS-1.8, A Nuclear Reaction Program*, NRG-1755 ZG (Petten, The Netherlands, 2015) `http://www.TALYS.eu`.
24. A.J. Koning, J.P. Delaroche, Nucl. Phys. A **713**, 231 (2003).
25. C. Kalbach, Phys. Rev. C **33**, 818 (1986).
26. R. Capote *et al.*, Nucl. Data Sheets **110**, 3107 (2009).
27. M. Wagner *et al.*, *Physik Daten-Physics Data, Evaluation of cross-sections for 14 important neutron dosimetry reactions* (Gesellschaft für wissenschaftlich-technische Information mbH, 1990).
28. S.M. Qaim, A. Mushtaq, M. Uhl, Phys. Rev. C **38**, 645 (1988).
29. N.I. Molla, S.M. Qaim, M. Uhl, Phys. Rev. C **42**, 1540 (1990).
30. S.M. Qaim *et al.*, Phys. Rev. C **42**, 363 (1990).
31. S. Sudár, F. Szelecsényi, S.M. Qaim, Phys. Rev. C **48**, 3115 (1993).
32. F. Cserpák *et al.*, Phys. Rev. C **49**, 1525 (1994).
33. I.G. Birn *et al.*, Phys. Rev. C **52**, 2546 (1995).
34. S. Sudár, S.M. Qaim, Phys. Rev. C **53**, 2885 (1996).
35. C.D. Nesaraja, S. Sudár, S.M. Qaim, Phys. Rev. C **68**, 024603 (2003).
36. S. Sudár, S.M. Qaim, Phys. Rev. C **73**, 034613 (2006).
37. M. Al-Abyad *et al.*, Phys. Rev. C **73**, 064608 (2006).
38. *RIPL-2 Reference Input Parameter Library* (IAEA, Vienna) `http://www-nds.iaea.org/RIPL-2/`.